

# Effect of Pre- and Postsynaptic Firing Patterns on Synaptic Competition

Nobuhiro Hinakawa<sup>(✉)</sup> and Katsunori Kitano

Department of Human and Computer Intelligence, Ritsumeikan University,  
1-1-1 Nojihigashi, Kusatsu, Shiga 5258577, Japan  
h@cns.ci.ritsumei.ac.jp, kitano@ci.ritsumei.ac.jp

**Abstract.** Synaptic plasticity is known to depend on the timing of pre and postsynaptic spikes, a.k.a. spike-timing-dependent plasticity (STDP). This implies that outcomes brought about by STDP should be sensitive to the dynamic properties of pre and postsynaptic neuron activity. Furthermore, because the classical model of STDP does not consider the effect of various pre and postsynaptic spike patterns on the outcome, it fails to reproduce the dependence of the synaptic plasticity polarity, namely the long-term potentiation or depression, on firing rates. In this study, we investigated the interplay between realistic pre and postsynaptic dynamic property models and a modified STDP model, reproducing the firing rate dependency. Our results showed that strengthened synapses depend on a combination of pre and postsynaptic properties as well as input firing rates, suggesting that a postsynaptic neuron may favor specific spike statistics and input firing rates may facilitate this tendency.

**Keywords:** STDP · Synaptic competition · Inter-spike intervals · MAT model

## 1 Introduction

Neurons in the brain connect with each other through a vast number of synapses responsible for neural information transfer. It is known that a synapse undergoes change in strength depending on the pre and postsynaptic neural activities, which is called Hebbian synaptic plasticity. In addition, it is supposed that this type of synaptic plasticity should be a neural substrate of higher-order functions, such as learning and memory.

The amount of change in synaptic strengths is determined by the timing of pre and postsynaptic spikes as well as their firing rates [1–3]. This suggests that the strengths should be sensitive to dynamic characteristics of pre and postsynaptic neurons. Indeed, a variety of spike statistic classes have been found, depending on the cortical regions and layers [4]. In most computational studies, however, theoretically-tractable assumptions have been imposed on such characteristics; presynaptic spike trains are characterized by a Poisson process whereas

postsynaptic spiking activity can be reproduced using the leaky integrate-and-fire (LIF) neuron model. A previous study introduced more realistic characteristics by using Gamma spike trains and the multi-timescale adaptive threshold (MAT) model [5, 6]. The results of the study showed that the outcomes of synaptic competition through spike-timing-dependent plasticity (STDP) depend on combinations of pre and postsynaptic characteristics [5]. However, the dependence of the outcomes on firing rates was inconsistent with known experimental evidence that high frequency inputs induce long-term potentiation (LTP), whereas low frequency inputs induce long-term depression (LTD). This result was due to the nature of the STDP model [7] used. Therefore, the outcome of the interplay between the characteristics of pre and postsynaptic activity, and the more realistic STDP rule, on reproducing the firing rate dependence is still unclear.

In our research, we addressed this issue by incorporating the STDP rule proposed by Pfister and Gerstner (2006) into the previous study [9]. The STDP rule takes into consideration additional synaptic spikes, not solely a pair of a pre and a postsynaptic spikes. This successfully reproduces the firing rate dependence. We investigated the type of features that are preferred and strengthened by pre and postsynaptic spikes through synaptic competition under the STDP rule defined by the time between spikes, which we term spike patterns.

## 2 Methods

### 2.1 Postsynaptic Neuron Model

The dynamics of the postsynaptic neuron can be represented by the MAT model, which reproduces cortical spike patterns more accurately than any other neuron model, such as LIF model [6]. The membrane potential  $V$  of the MAT model obeys the following linear differential equation

$$\tau_m \frac{dV}{dt} = V_{\text{rest}} - V + \sum_i^{1000} g_i^{\text{ex}}(t) (E_{\text{ex}} - V) + \sum_i^{200} g_i^{\text{in}}(t) (E_{\text{in}} - V), \quad (1)$$

where  $\tau_m$ ,  $V_{\text{rest}}$ ,  $E_{\text{ex}}$ , and  $E_{\text{in}}$  are the membrane time constant, the resting membrane potential, and the reversal potential of excitatory and inhibitory synapses, respectively.  $g_i^{\text{ex}}(t)$  and  $g_i^{\text{in}}(t)$  are the conductance of the  $i$ th excitatory synapse and the  $i$ th inhibitory synapse, respectively. In addition, when the membrane potential  $V$  reaches the time-varying threshold  $\theta(t)$ , the neuron generates a neural spike without resetting the membrane potential.  $\theta(t)$  is described in time as follows:

$$\theta(t) = \omega + \sum_l (\alpha_1 e^{-(t-t_l)/\tau_1} + \alpha_2 e^{-(t-t_l)/\tau_2}), \quad (2)$$

where  $\alpha_j$  and  $\tau_j$  are the amount and the decay time constants of the threshold increase, respectively.  $\omega$  is the time-invariant threshold. Each time-varying component of  $\theta(t)$  increases simultaneously at spike time  $t_l$  by  $\alpha_1$ ,  $\alpha_2$  and then exponentially decays.

## 2.2 Synapse Model

The dynamics of the synaptic conductance is modeled by

$$\frac{dg_i^X}{dt} = -\frac{g_i^X}{\tau_X} + \hat{g}_i^X \sum_l \delta(t - t_l) \quad (X = \text{ex, in}), \quad (3)$$

where  $\tau_X$ ,  $\hat{g}_i^X$ , and  $\delta(\cdot)$  are the time constant, the peak synaptic conductance, and the Dirac's delta function, respectively. While the peak conductance of inhibitory synapses was constant, the excitatory synapses changed according to the following description:

$$\hat{g}_i^{\text{ex}} \rightarrow \hat{g}_i^{\text{ex}} + g_{\max} w_i(t), \quad (4)$$

where  $g_{\max}$  is the maximal synaptic conductance and  $w(t)$  defines an amount of synaptic plasticity. To implement the STDP rule in our study, a triplet-based model with all-to-all interactions was used [9], in which the variable  $w(t)$  changed as described below. The presynaptic spike, generated at time  $t_{\text{pre}}$ , triggers a change depending on the postsynaptic variable  $o_1$  and the second presynaptic variable  $r_2$  as follows:

$$w(t) \rightarrow w(t) - o_1(t) [A_2^- + A_3^- r_2(t - \epsilon)]. \quad (5)$$

Similarly, the postsynaptic spike, generated at time  $t_{\text{post}}$ , triggers a change depending on the presynaptic variable  $r_1$  and the second postsynaptic variable  $o_2$  as follows:

$$w(t) \rightarrow w(t) + r_1(t) [A_2^+ + A_3^+ o_2(t - \epsilon)]. \quad (6)$$

$A_2^-$  and  $A_2^+$  are the weight change amplitudes whenever there is a post-pre pair and pre-post pair, respectively. Similarly,  $A_3^-$  and  $A_3^+$  are the triplet term amplitudes for depression and potentiation, respectively. If a presynaptic spike is generated, the presynaptic detectors  $r_1$  and  $r_2$  are updated by  $r_1 = r_1 + 1$  and  $r_2 = r_2 + 1$ . Otherwise, the presynaptic detectors  $r_1$  and  $r_2$  decay in the following manner:

$$\frac{dr_1(t)}{dt} = -\frac{r_1(t)}{\tau_+}, \quad (7)$$

$$\frac{dr_2(t)}{dt} = -\frac{r_2(t)}{\tau_x}. \quad (8)$$

Similarly, if a postsynaptic spike is generated, the postsynaptic detectors  $o_1$  and  $o_2$  are updated by  $o_1 = o_1 + 1$ , and  $o_2 = o_2 + 1$ . Otherwise, the postsynaptic detectors  $o_1$  and  $o_2$  decay exponentially.

$$\frac{do_1(t)}{dt} = -\frac{o_1(t)}{\tau_-}, \quad (9)$$

$$\frac{do_2(t)}{dt} = -\frac{o_2(t)}{\tau_y}. \quad (10)$$

$\tau_+$ ,  $\tau_x$ ,  $\tau_-$ , and  $\tau_y$  are the time constants of the corresponding variables.

### 2.3 Presynaptic Spike Trains

Inter-spike intervals (ISIs) of a presynaptic spike train obey a gamma distribution. An ISI  $T_l = t_l - t_{l-1}$  was drawn from a gamma distribution;

$$T_l \sim p(T; k, \lambda) = \frac{\lambda^k T^{k-1} e^{-\lambda T}}{\Gamma(k)}. \quad (11)$$

$k$  is the shape parameter,  $\lambda$  is the rate parameter, and  $\Gamma(k)$  is the gamma function. The mean ISIs,  $\bar{T}$ , is  $\bar{T} = \frac{k}{\lambda}$ . The shape parameter  $k$  defines the shape of the distribution. If  $k = 1$ , the distribution is an exponential distribution generating a Poisson spike train. The presynaptic spike train shows nearly periodic firing for larger  $k$ , whereas it shows burst firing for a smaller  $k(<1)$ .

### 2.4 Numerical Simulations

In order to examine how synaptic competition is affected by interplay between presynaptic inputs and postsynaptic dynamics, we compared different combinations of pre and postsynaptic characteristics. Input spikes were generated by the gamma distribution with various values for the shape parameter. The LIF and MAT models were implemented to represent the postsynaptic neuron (results shown below are obtained using the MAT model). In our final investigation, 1,000 excitatory synapses were divided into 4 subgroups (250 synapses per a subgroup). Synapses in each subgroup delivered spike trains generated by gamma distributions with an identical shape parameter; the parameter for the  $i$ -th group was set to  $k = 2^{i-1}$ .

The parameters of the MAT model were the same as those used in a previous study [5]. Other model parameters were taken from another previous study [9].

## 3 Results

For various input firing rates, we conducted numerical simulations using our computational model until the distribution of synaptic strengths reached a stationary state. We focused on the stationary distribution of synaptic strengths and postsynaptic firing characteristics, firing rate, and coefficients of variation (Cv) of the postsynaptic neuron ISIs, as a function of the presynaptic spike trains.

### 3.1 Inputs with an Identical Value of $k$

We first examined synaptic competition in the case where input spike trains were generated by a gamma distribution with identical shape parameter values ( $k = 1$ ) for all excitatory synapses. Figure 1 shows the stationary distribution of synaptic strengths for various input firing rates and the spike statistics of the postsynaptic neurons in the stationary state. Figures 1a–d show that all distributions exhibited bimodal shapes, in which there existed two populations

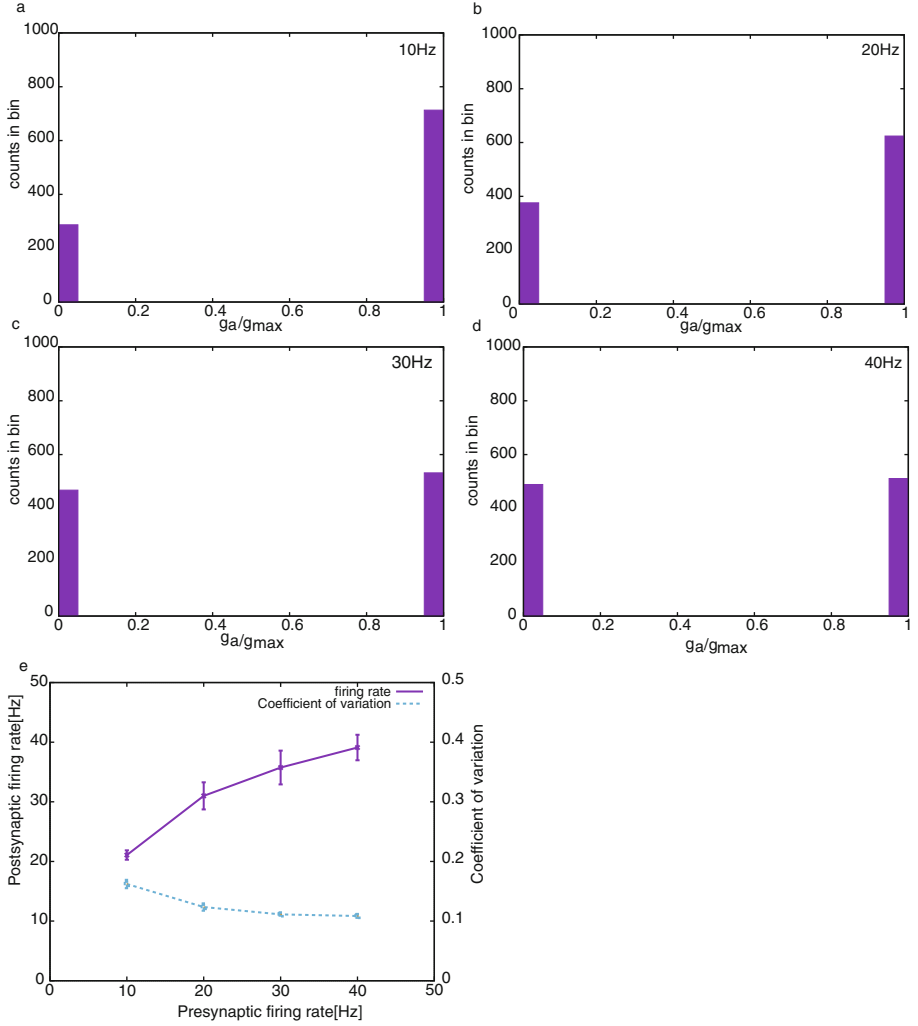


**Fig. 1.** Synaptic competition and activity regulation when the MAT model received Poisson spike trains ( $k = 1$ ). **a.** Stationary distributions of synaptic strengths for an input firing rate of 10 spikes/s. The abscissa indicates the normalized synaptic conductance. **b**, **c**, and **d** are similar to **a**, but for 20 spikes/s, 30 spikes/s, and 40 spikes/s, respectively. **e.** Dependencies of postsynaptic firing rates and coefficients of variation (Cv) of postsynaptic ISIs on the input firing rates.

of strengthened synapses (around 1) and weakened synapses (around 0). As the input firing rate was increased, the population of strengthened synapses became smaller, and the population of weakened ones became larger. However, the change in the fraction of the two populations could be seen with an increase in the input firing rate of up to 30 spikes/s. Figure 1e shows the postsynaptic

firing rate and coefficients of variation (Cv) of the postsynaptic ISIs. The firing rate of postsynaptic neurons increased moderately, suggesting that the activity regulation by the STDP was successful, but weak. The Cv of postsynaptic ISIs were kept low due to the dynamic nature of the MAT model.

Figures 2a–d show the mean synaptic conductances as a function of the input firing rate for various values of the shape parameter ( $k = 0.5, 1, 4$ , and  $8$ ). When  $k = 0.5$  and  $1$ , averaged synaptic strengths monotonically decreased with an increase in input firing rates. In contrast, for  $k = 4$  and  $8$ , they differently depended on the input firing rates, suggesting that the interplay between the postsynaptic dynamics and the input spike patterns modulated the process of synaptic competition.

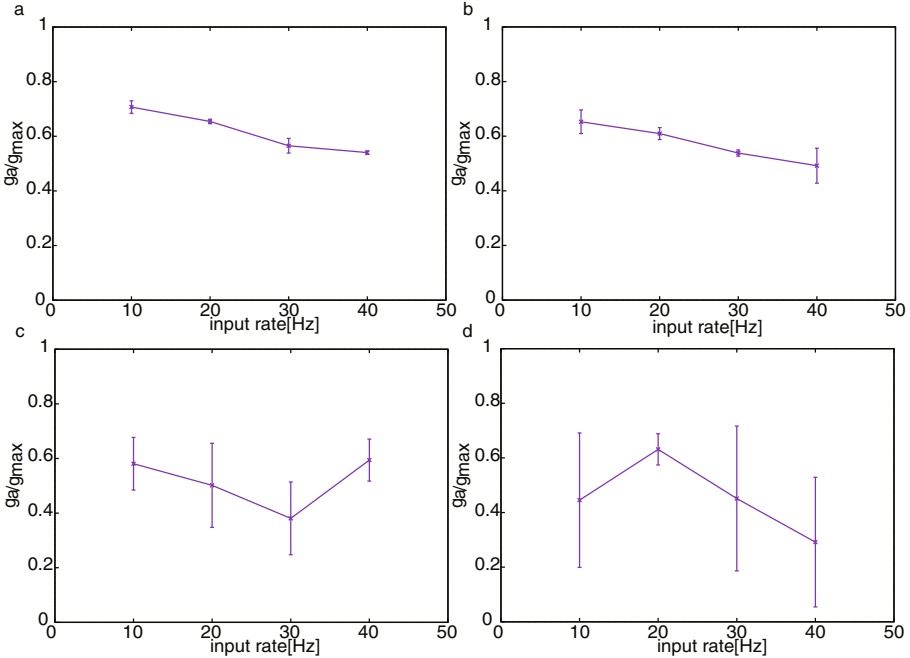


**Fig. 2.** Averaged synaptic strengths when the MAT model received Gamma spike trains. **a.** The averaged synaptic strengths if input spikes were generated by the Gamma distribution with  $k = 0.5$  and various input firing rates. The abscissa axis indicates the input firing rate. **b**, **c**, and **d** are similar to **a**, but for  $k = 1$ ,  $k = 4$ , and  $k = 8$ , respectively.

### 3.2 Inputs with Different Values of $k$

Next, in order to see if synapses delivering a specific spike train were selectively potentiated, we examined synaptic competition in the case where input spikes were generated by a mixture of spike trains with different regularity (see Methods). While synapses in the subgroup 1 provided spike trains with  $k = 1$ , namely

Poisson spike trains, those in subgroup 4 did so with more regular spike trains. Figure 3a shows averaged synapse strengths within a subgroup for different input firing rates. For the lower input firing rates (*le* 20 spikes/), the averaged synaptic strengths for the subgroup with a smaller  $k$  seemed more increased. In contrast, for increased input firing rates ( $\geq 30$  spikes/s), synapses in the subgroup with a larger  $k$  was likely to be more potentiated. In Fig. 3b, the postsynaptic firing rate and coefficients of variation (Cv) of postsynaptic ISIs are shown as a function of the input firing rate. The change in the postsynaptic firing rate was similar to that in Fig. 1, and activity regulation worked moderately for this condition as well. However, the ISI Cvs decreased with an increase in the input firing rate.

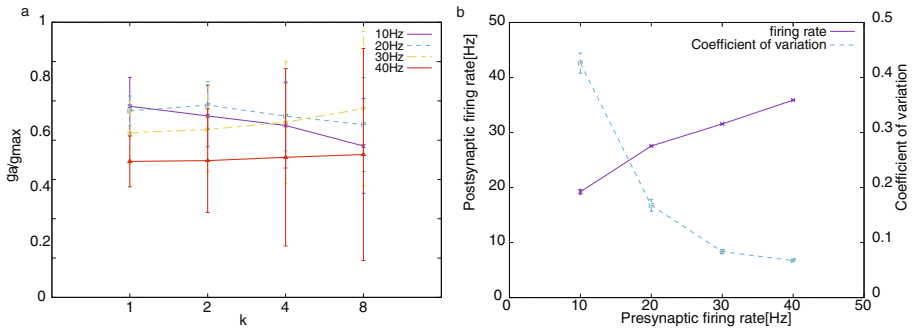


**Fig. 3.** Synaptic strengths and postsynaptic spike statistics when the MAT model received a mixture of Gamma spike trains with different regularity ( $k = 1, 2, 4$ , and  $8$ ). **a.** The averages of synaptic strengths within a subpopulation for various input firing rates. The abscissa indicates the values of the shape parameter  $k$ . **b.** Dependencies of postsynaptic firing rates and coefficients of variation (Cv) of postsynaptic ISIs on the input firing rates.

## 4 Discussion

If the shape parameter  $k$  is identical for all input spike trains, we obtain results similar to those in the previous study. Both methodologies give the distribution of synaptic strengths, the shift between strengthened and weakened populations with an increase in input firing rates, and a moderate increase in the postsynaptic firing rate [7]. Thus, employing the STDP rule did not cause differences under this condition.

However, in the case of mixture spike trains with different spike patterns ( $k$ ), the STDP rule could strengthen the synapses delivering spike trains with larger  $k$ , that is, more periodic spike trains with an increase in the input firing rate. If the dynamics of the postsynaptic neuron was modeled by the LIF neuron, such a preference was not seen for any input firing rates (data not shown). These results suggest that the determination of which synapses are potentiated is determined by a combination of the presynaptic spike train structure ( $k$ ) and the dynamic property of the postsynaptic neuron (This is found using either the LIF or MAT models).

Thus, we conclude (i) the dynamic feature of postsynaptic neurons could favor a specific spike pattern through synaptic competition brought about by STDP and (ii) such a preference depends on input firing rates. Although the former conclusion was already obtained by the previous study applying the classical STDP rule [5, 7], the latter was achieved only through our use of the employed STDP rule.

## References

1. Markram, H., Lubke, J., Frotscher, M., Sakmann, B.: Regulation of synaptic efficacy by coincidence of postsynaptic APs and EPSPs. *Science* **275**, 213–215 (1997)
2. Bi, G.-Q., Poo, M.-M.: Synaptic modifications in cultured hippocampal neurons: dependence on spike timing, synaptic strength, and postsynaptic cell type. *J. Neurosci.* **18**, 10464–10472 (1998)
3. Bliss, T.V., Lomo, T.: Long-lasting potentiation of synaptic transmission in the dentate area of the anaesthetized rabbit following stimulation of the perforant path. *J. Physiol.* **232**, 331–356 (1973)
4. Shinomoto, S., Miyazaki, Y., Tamura, H., Fujita, I.: Regional and laminar differences in in vivo firing patterns of primate cortical neurons. *J. Neurophysiol.* **94**, 567–575 (2005)
5. Ito, H., Kitano, K.: Pre- and postsynaptic properties regulate synaptic competition through spike-timing-dependent plasticity. In: Wermter, S., Weber, C., Duch, W., Honkela, T., Koprinkova-Hristova, P., Magg, S., Palm, G., Villa, A.E.P. (eds.) ICANN 2014. LNCS, vol. 8681, pp. 733–740. Springer, Heidelberg (2014)
6. Kobayashi, R., Tsubo, Y., Shinomoto, S.: Made-to-order spiking neuron model equipped with a multi-timescale adaptive threshold. *Front. Comput. Neurosci.* **3**, 9 (2009)
7. Song, S., Miller, K.D., Abbott, L.F.: Competitive Hebbian learning through spike-timing-dependent synaptic plasticity. *Nat. Neurosci.* **3**, 919–926 (2000)
8. Cateau, H., Fukai, T.: A stochastic method to predict the consequence of arbitrary forms of spike-timing-dependent plasticity. *Neural Comput.* **15**, 597–620 (2003)
9. Pfister, J.P., Gerstner, W.: Triplets of spikes in a model of spike-timing-dependent plasticity. *J. Neurosci.* **26**, 9673–9682 (2006)

Artificial Neural Networks and Machine Learning – ICANN  
2016

25th International Conference on Artificial Neural  
Networks, Barcelona, Spain, September 6-9, 2016,  
Proceedings, Part I

Villa, A.E.P.; Masulli, P.; Pons Rivero, A.J. (Eds.)

2016, XXIX, 567 p. 195 illus., Softcover

ISBN: 978-3-319-44777-3